THE ASTRONOMICAL JOURNAL, 117:1441–1453, 1999 March

WIND INHOMOGENEITIES IN WOLF-RAYET STARS. III. UNUSUAL EMISSION-LINE PROFILE VARIATIONS IN γ^2 VELORUM

SÉBASTIEN LÉPINE,[1,2] THOMAS EVERSBERG,[1] AND ANTHONY F. J. MOFFAT[1,3]
Département de Physique, Université de Montréal, C.P. 6128, Succursale Centre-Ville, Montréal, QC H3C 3J7, Canada, and Observatoire du Mont-Mégantic; lepine@stsci.edu, eversber@astro.umontreal.ca, moffat@astro.umontreal.ca
Received 1998 July 27; accepted 1998 November 30

ABSTRACT

We present very high resolution, very high signal-to-noise ratio spectra from the 3.6 m Canada-France-Hawaii telescope for the strong C III λ5696 emission line in γ^2 Velorum, the brightest Wolf-Rayet (WR) star in the sky. From two nights of spectroscopic monitoring, we have detected line profile variations (LPVs) in the form of moving emission features (subpeaks) on the broad, "flat-topped" underlying profile. We use the working model from the previous paper in this series to study these LPVs in terms of inhomogeneities in the radially expanding stellar wind. A comparison between simulations and the data suggests the variable subpeaks to consist of a superposition of two distinct components: (1) narrow-moving subpeaks with a mean line-of-sight velocity dispersion $\overline{\sigma}_\xi \simeq 80$ km s^{-1}, and (2) broad-moving subpeaks with $\overline{\sigma}_\xi \simeq 200$ km s^{-1}. Both narrow and broad subpeak components are seen to move systematically in a direction from the line center ($\xi = 0$) toward the line edges. This motion is found to be consistent with a radial wind expansion at a mean acceleration rate $a_r = 13 \pm 3$ m s^{-2}. The narrow subpeaks are found to be similar to the stochastic subpeaks seen in the LPVs from several single and long-period binary WR stars. On the other hand, the broad features are reminiscent of the recurrent subpeaks observed in the LPVs from a few peculiar WR stars (HD 4004, HD 191765, and EZ CMa), although in γ^2 Vel, we find no evidence for a recurrent behavior.

We investigate the possibility that, in γ^2 Vel, these broad variable subpeaks arise from the shock-cone region, at the interface where the wind from the WR star collides with that of its O companion. We find no convincing evidence to support this hypothesis, although we suspect that there could be a relation between the existence of broad LPV subpeaks and the presence of the more massive O companion.

Key words: methods: data analysis — stars: individual (γ^2 Velorum) — stars: Wolf-Rayet

1. INTRODUCTION

Wolf-Rayet (WR) stars are believed to be the evolved counterparts of massive OB stars (Pasquali et al. 1997). They are characterized by intense mass loss occurring through dense, fast winds ($\dot{M} \sim 10^{-5}\ M_\odot$ yr^{-1}; $v_\infty \sim 10^3$ km s^{-1}), consisting mainly of products from the CNO cycle for stars in the WN sequence (Hamann et al. 1994) and of products from the triple-α cycle for stars of the WC sequence (Grafener et al. 1998). The optical spectra of WR stars typically show broad emission lines from these elements. The broad recombination lines are believed to arise from the radial expansion and subsequent cooling of the wind (e.g., Schmutz 1997).

For simplicity, hot winds from WR stars have traditionally been modeled as steady, homogeneous flows. Until recently, models used in the spectral analysis of WR winds depended on a set of simplifying assumptions grouped under the name of *standard model* for WR stars (see Langer 1989). In this standard model, the wind is assumed to be (1) spherically symmetric; (2) radially expanding with a monotonic velocity law; (3) homogeneous; and (4) time-independent, or steady. However, the theory of radiation-driven winds predicts that WR winds should be hydrodynamically unstable (e.g., Owocki & Rybicky 1991), and theoretical models suggest that this leads to the development of strong wind clumping (Gayley & Owocki 1995).

Investigation of wind clumping mainly comes from indirect observational evidence. These include the low intensity in the electron scattering wings of wind emission lines (Hillier 1991), IR emission-line ratios (Nugis & Niedzielski 1995), stochastic variations in polarized light (Robert et al. 1989), and continuum excess in IR and radio free-free emission (Runacres & Blomme 1996). In all cases the inhomogeneity is observed by the way it *globally* affects the emission from the stellar wind. Although such observations may provide estimates of the *clumping factor*, i.e., the amplitude in the density fluctuations in the flow, they provide little information on the detailed geometry of the inhomogeneous structure.

Though it might be possible in the near future to resolve the inhomogeneous wind structure using optical interferometry (e.g., Vakili et al. 1997), no direct imaging of detailed WR wind structure is currently available. Details about the clumpy structure can, however, be obtained from high-resolution spectroscopy of wind emission lines. Because the wind velocity in WR stars is very high ($v_\infty \sim 10^3$ km s^{-1}), wind regions having different line-of-sight velocities can be spectroscopically resolved (cf. Lépine & Moffat 1999; hereafter Paper II). Monitoring of optical lines in several WR stars has revealed the presence of significant levels of line profile variations (LPVs) on timescales of minutes to days, which can be interpreted as variations in the wind density structure. We can classify the observed LPVs in three types: narrow, stochastic subpeaks (S-type); broad, recursive subpeaks (R-type); and periodic line modulations (P-type).

S-type LPVs show up as variable subpeak features with mean line-of-sight velocity dispersion $\overline{\sigma}_\xi \sim 100$ km s^{-1} (Robert 1992; Lépine et al. 1996, hereafter Paper I). These

[1] Visiting Astronomer, Canada-France-Hawaii Telescope.
[2] Now at the Space Telescope Science Institute, 3700 San Martin Drive, Baltimore, MD 21218.
[3] Killam Research Fellow of the Canada Council for the Arts.

are systematically observed to move away from the line center, i.e., features on the $\xi < 0$ side of the line move toward the blue edge, while features on the $\xi > 0$ side move toward the red edge (Moffat et al. 1988). Variable features were shown to persist on timescales of ~ 8 hours (Paper II), but any search for periodic or recursive behavior has so far been negative. The subpeaks are, therefore, assumed to be stochastic in nature and are believed to be the trace signature of local wind inhomogeneities. This type of LPV seems to be omnipresent in hot stellar winds. Apart from their detection in at least eight other WR stars, either single or in long-period binaries (Robert 1992; Paper II), S-type LPVs have also been detected in central stars of planetary nebula (BD $+30°3639$, Acker et al. 1997; NGC 40, Balick et al. 1996) and in one Of star (ζ Pup, Eversberg et al. 1998a).

R-type LPVs appear as broader ($\overline{\sigma}_\xi \sim 200$–$500$ km s^{-1}) subpeak features that move across the line profile and typically persist for ~ 10 hours. Apart from their larger width, they sometimes look like S-type LPVs. However, their variation patterns are found to be *recursive* on timescales of a few days (McCandliss et al. 1994). They have been found in a few apparently peculiar WR stars: HD 191765 (Vreux et al. 1992; Morel et al. 1998), EZ CMa (St.-Louis 1995; Morel et al. 1997), and HD 4004 (Morel et al. 1998). Several interpretations have been suggested to explain this phenomenon, including the presence of a compact companion hidden in the wind (Drissen et al. 1989), a bipolar jet (Vreux et al. 1992), or a wind surface connection (Morel et al. 1997).

P-type LPVs occur in the form of dramatic (greater than 10% of line emission) variations in the shape of the line profile, which are correlated with the orbital period in binary WR + O systems (St.-Louis et al. 1996; Moffat 1996). Some of these phase-dependent LPVs can be modeled as excess line emission from the wind-wind collision zone between the two hot-star components (Marchenko et al. 1995; Luehrs 1997). Other periodic variations were explained as selective eclipses of one star by the wind of its stellar companion (St.-Louis 1993).

In the previous two papers in this series, we have investigated S-type LPVs with the use of a simple phenomenological model in which the LPVs arise from local inhomogeneities in a radially expanding stellar wind. This working model uses the idea that an emission line arising from a clumped wind can be though of as arising from the sum of a large number of discrete wind emission elements (DWEEs). With a few assumptions about the statistical distribution and relative emission of individual DWEEs as a function of time, we have obtained simulations that agree with the data remarkably well.

A comparison of these synthetic LPV patterns with observations of LPVs in optical WR emission lines yielded several constraints on the inhomogeneous structure of WR winds. We found that the wind must consist of a huge number ($N_e \gtrsim 10^4$–10^5) of DWEEs. These DWEEs must have large, intrinsic velocity dispersions $\overline{\sigma}_v \sim 100$ km s^{-1} to account for the size of variable subpeaks in the line-of-sight velocity space ξ. There is strong evidence for the local velocity dispersion within DWEEs to be anisotropic, with $\sigma_{v_r} \sim 4\sigma_{v_\theta}$, where σ_{v_r} is the velocity dispersion along the propagation axis (radial), while σ_{v_θ} is the velocity dispersion perpendicular to the propagation axis. The radial acceleration rates of DWEEs, $a_r \sim 5$–30 m s^{-2}, are found to be smaller than the wind acceleration predicted from the standard model of WR stars ($a_r \gtrsim 50$ m s^{-2}). The duration of subpeak events is found to be consistent with the time it takes for a local wind inhomogeneity to pass through the line-emission region.

We also reported in Papers I and II on observational limits in the study of inhomogeneous WR wind structure from LPVs in their optical emission lines. We suggested that one would benefit from using very high spectral resolution and signal-to-noise ratio, combined with a very tight and extensive time sampling, in order to uncover important details in the patterns of LPV. It turns out that the best star for such a study is the very bright WR star γ^2 Velorum, with apparent visual magnitude $V \simeq 1.82$. Even though γ^2 Vel owes this brightness partly to its O-type companion, it is still by far the closest WR star (van der Hucht et al. 1997; Schaerer et al. 1997). If it were a single WR star, it would shine with $V \simeq 3.2$.

This paper presents a series of very high resolution spectra of γ^2 Vel obtained from the Canada-France-Hawaii telescope (§ 2). The observed LPV patterns are analyzed with the help of a multiscale analysis method involving the wavelet transform (§ 3). The data are compared with LPV simulations from a model of radially propagating inhomogeneous wind features (§ 4). It is shown that the data can be accounted for by the existence of two separate LPV modes, one consisting of the usual stochastic, narrow emission subpeaks, the other one arising from an additional component of broad subpeaks, which are similar to R-type LPVs, although no recursive behavior has been confirmed yet. The results are discussed in § 5, where we discuss the possible origin of the broad LPV subpeaks. A summary follows in § 6.

2. OBSERVATIONS AND REDUCTION

On heliocentric Julian dates (JD) 2,450,061 and 2,450,063 we observed γ^2 Velorum at the Coudé focus of the Canada-France-Hawaii 3.6 m telescope on Mauna Kea. We used the 1800 l mm^{-1} holographic grating to project spectral images with the f/8 camera onto a Reticon 1872 array detector with 75 μm $\times$ 15 μm pixels. We monitored the strong C III λ5696 optical emission line with successive, short (300 s) exposures, achieving a signal-to-noise ratio S/N ~ 2000 pixel^{-1}, and a 2.5 pixel resolution of $\Delta\lambda \sim 0.08$ Å. This was equivalent to monitoring at 5696 Å with a line-of-sight velocity resolution $\Delta\xi \simeq 4.2$ km s^{-1}.

Reduction was carried out using IRAF with the Reticon reduction package developed by D. Bohlender and G. Hill, which includes the baseline reduction, flat-fielding, heliocentric correction, and wavelength calibration with a ThAr comparison spectrum. The whole C III λ5696 emission line is so broad in γ^2 Vel that it could not all fit in the full 58 Å range available at the detector. Thus, the extreme blue and red line wings do not appear in the data images. The absence of a flat continuum region means that we had to rectify the spectra by fitting a straight line passing through fixed wavelength regions on the blue and red edges, where contributions from the line emission are minimal. Although this means that precise estimates of equivalent widths cannot be obtained from our data, our analysis of LPVs should not be significantly affected.

One single night of data consists of N spectra taken at times t_i ($i = 1, \cdots, N$). The spectra can be denoted as a spectral time series $S(\xi, t_i)$, where $\xi = (\lambda - \lambda_0)\lambda_0^{-1} c$ is the line-of-sight Doppler velocity of line-emitting atoms, with $\lambda_0 = 5696$ Å. We define the residual spectra $R(\xi, t_i)$ as the

instantaneous deviation from the mean profile:

$$R(\xi, t_i) = S(\xi, t_i) - \frac{1}{N} \sum_{i=1}^{N} S(\xi, t_i) \, . \quad (1)$$

The time series of residual spectra are presented for each night in Figure 1, along with the mean profile and the maximum and minimum values recorded in $S(\xi, t_i)$ for each pixel element. We detect variability in the line on timescales of minutes to hours, with a mean amplitude $\sim 5\%$ of the continuum level, i.e., about 50 times larger than the expected instrumental noise. Fluctuations do not occur independently from pixel to pixel, but rather appear in the form of extended features in line-of-sight velocity space ξ.

The variations also seem to follow a systematic trend. The intensity in some sectors seems to increase systematically during the night, whereas it apparently decreases in other sectors. This gives one the impression that the variations occur in the form of excess features that are either in emission or absorption, and that emission features gradually turn to absorption in the course of the night and vice versa. However, we can show these apparent reversal patterns to be numerical artifacts. Although the level of reference $\overline{S}(\xi)$ is well defined for each night, it is still arbitrary; the fact that one feature appears in emission or absorption in $R(\xi, t_i)$ has no direct physical meaning. The procedure in equation (1) can also introduce spurious features in $R(\xi, t_i)$ if $\overline{S}(\xi)$ is not perfectly smooth. Furthermore, values of $R(\xi, t_i)$ always add up to zero at any wavelength when summed over t_i, as is evident from equation (1). This means that slow, systematic variations in the line profile will always produce inversion patterns like those observed in Figure 1.

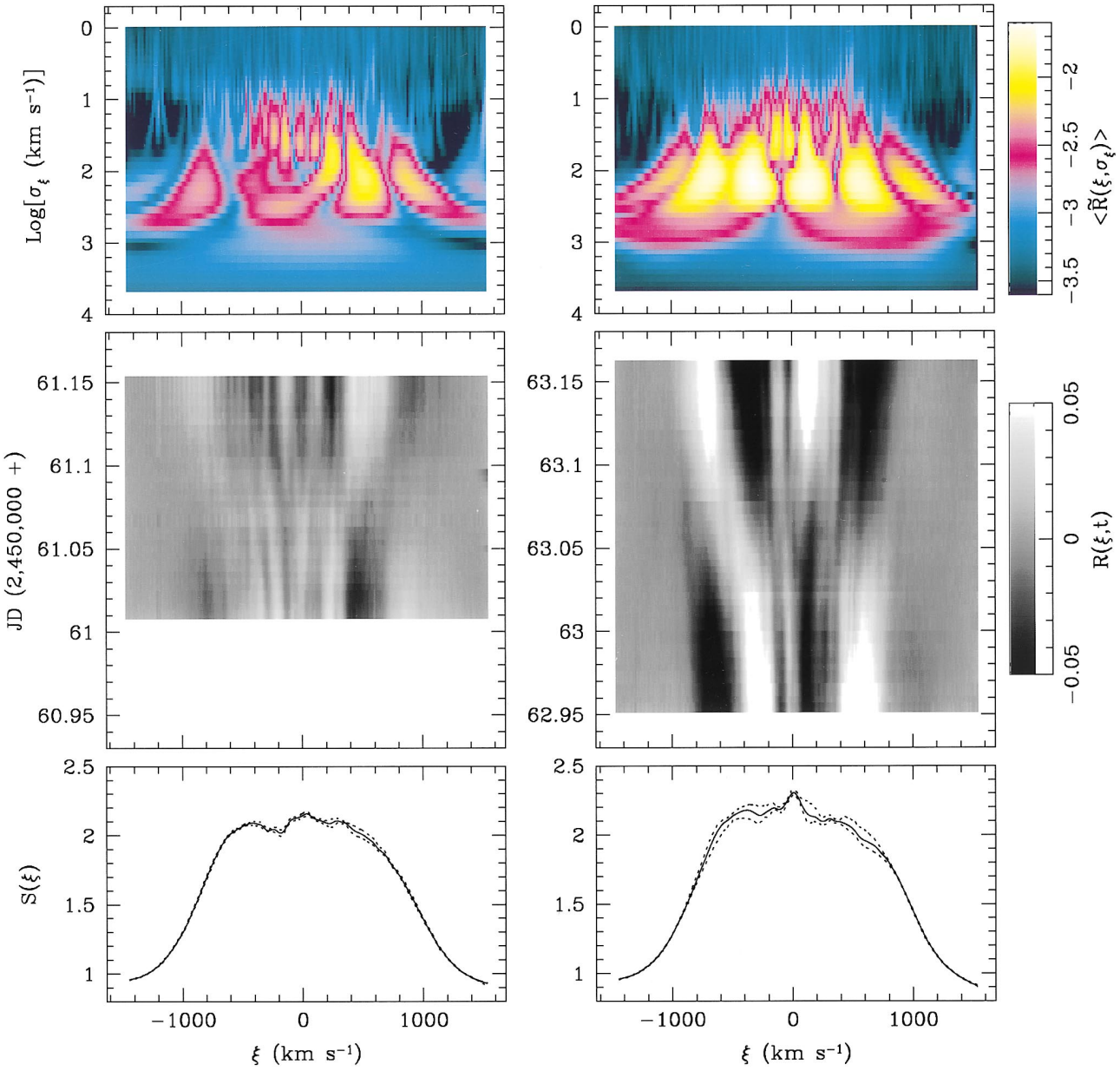

FIG. 1.—Spectral time series of the residuals $R(\xi, t_i)$ in the C III λ5696 emission line (gray-scale plots) (*middle*) obtained after subtracting off the mean line profile, which is shown in the bottom panels (*solid line*) along with the maximum and minimum measured values (*dashed lines*). The color displays (*top*) show the mean wavelet spectrum for each time series (see § 3.1). The wavelet spectrum indicates the characteristic location (ξ) and scale (σ_ξ) of the variable line subpeaks.

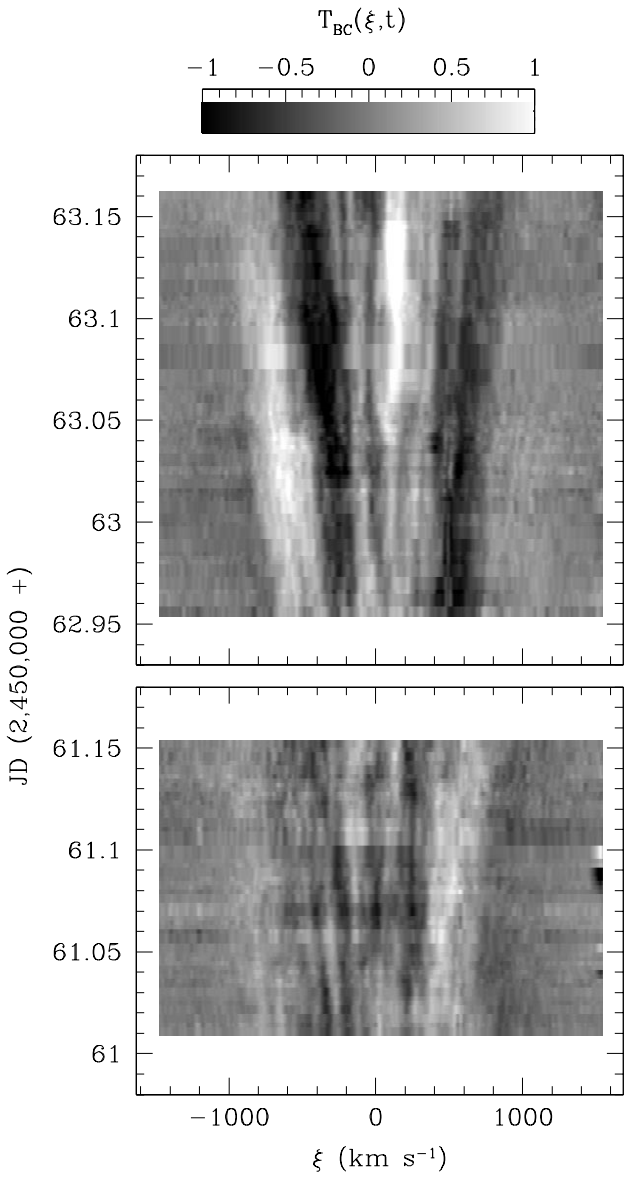

FIG. 2.—Instantaneous variation with time, $T(\xi, t_i)$, in the spectral time series, obtained by comparison of successive spectra. This yields a more objective representation for the time variability in the emission line than do the residuals, because $R(\xi, t_i)$ is dependent on the arbitrary choice of the mean spectrum. The plots clearly shows that LPVs consist of features that systematically move from the line center ($\xi = 0$) toward the line edges, whereas the gray-scale plots in Fig. 1 did not show this behavior unambiguously.

For example, an excess emission feature at the start of the series will always be followed by an apparent absorption through.

Systematic variations in the spectrum can be better appreciated if we plot the *instantaneous* line variation gradient at any time. We define an instantaneous spectral variation gradient time series $T(\xi, t_j)$ as

$$T(\xi, t_j) \equiv \frac{S(\xi, t_p) - S(\xi, t_q)}{t_p - t_q} \tag{2}$$

for all

$$t_j = \frac{t_p + t_q}{2}, \quad \Delta t_{\min} < t_p - t_q < \Delta t_{\max},$$

that is, the difference between all pairs of spectra in the time series that are separated by a time interval $\Delta t_{\min} < \Delta t < \Delta t_{\max}$. This time interval should be selected in such a way that $\Delta t_{\max}$ is not too large as compared with $\Delta t_{\min}$, e.g., in order that one compares spectrum 1 with 3, 2 with 4, 3 with 5, etc. One drawback of this method is that it emphasizes the effects of instrumental noise, especially the random pixel-to-pixel variations. One way to minimize these effects is to use a $\Delta t_{\min}$ such that the mean amplitudes of LPVs after an interval $\Delta t \simeq \Delta t_{\min}$ are significantly larger than the standard deviation from the noise. Alternatively, we may use the wavelet filtering technique, described in § 3.2, to reduce the amplitudes of the pixel-to-pixel variations in the spectra. Figure 2 shows the $T(\xi, t_j)$ of the data (with $[\Delta t_{\min}, \Delta t_{\max}] = [6, 12]$ minutes), after having performed a wavelet filtering procedure with combined filters B and C (cf. § 3.2).

The resulting $T_{BC}(\xi, t_j)$ reveal that the LPV features systematically move from line center toward line edges. This pattern is consistent with LPVs arising from radially accelerating emission elements (see Moffat et al. 1988; Robert 1992; and Paper II). The LPV patterns in γ^2 Vel therefore behave similarly to the stochastic subpeaks observed in single, and long-period binary WR stars, which are interpreted in terms of inhomogeneities in a radially expanding stellar wind. The reason why one did not need to calculate the $T(\xi, t_j)$ in most previous studies is due to the greater time coverage leading to a more robust time average $\bar{S}(\xi)$.

3. MULTISCALE ANALYSIS

3.1. *Wavelet Spectrum*

We use wavelet analysis to quantify the characteristic scale and location of variable features in the spectra. A mathematical formulation and interpretation for the wavelet technique applied to spectral time series can be found in Papers I and II. The continuous *wavelet transform* over ξ of a data set $R(\xi, t_i)$, denoted $\tilde{R}(\xi, \sigma_\xi, t_i)$ is defined as

$$\tilde{R}(\xi, \sigma_\xi, t_i) \equiv \frac{\pi}{8} \int_{-\infty}^{\infty} R(\xi', t_i) \psi\left(\frac{\xi' - \xi}{\sigma_\xi}\right) \frac{d\xi'}{\sigma_\xi}, \tag{3}$$

where we use $\psi(x) = (1 - x^2) \exp -x^2/2$, the so-called Mexican hat function, as the wavelet. We also define the *mean wavelet power spectrum*, denoted $\langle \tilde{R}(\xi, \sigma_\xi) \rangle$, which combines the information from N individual spectra in the time series:

$$\langle \tilde{R}(\xi, \sigma_\xi) \rangle^2 \equiv \sum_{i=1}^{N} \frac{1}{N} [\tilde{R}(\xi, \sigma_\xi, t_i)]^2 . \tag{4}$$

The mean wavelet spectrum $\langle \tilde{R}(\xi, \sigma_\xi) \rangle$ shows the typical amplitude of variable features with a characteristic scale σ_ξ at each location ξ.

The mean wavelet spectrum for each of the two spectral time series from γ^2 Vel are displayed in Figure 1. The small-scale regime [$0 \lesssim \log \sigma_\xi(\text{km s}^{-1}) \lesssim 1$] shows a more or less uniform response over ξ and is the scale domain for pixel-to-pixel fluctuations. On intermediate scales [$1 \lesssim \log \sigma_\xi(\text{km s}^{-1}) \lesssim 3$], one sees a response in ξ whose intensity is correlated with the intensity of the emission line; this is the realm of *intrinsic* variable line features. The largest scale domain [$3 \lesssim \log \sigma_\xi(\text{km s}^{-1}) \lesssim 4$] is sensitive to variations on a scale comparable to the data interval, such as global line variations or continuum variations. Because of

the normalization procedure in the data reduction, these latter variations have been attenuated, which might explain the negligible wavelet response on that scale domain.

The wavelet spectrum reveals the existence of relatively narrow variable features near the line center ($\xi \sim 0$), which are absent near the line edges. This makes the wavelet spectra in Figure 1 look like semicircles centered on $\xi = 0$. This particular behavior has been observed to occur systematically in WR emission lines with S-type LPVs (see Paper II). It was interpreted as evidence for anisotropic velocity dispersion in the wind, with velocity dispersions in the radial direction larger than in the azimuthal direction ($\sigma_{v_r} \sim 4\sigma_{v_\theta}$). The LPVs in γ^2 Vel therefore show similarities with the S-type phenomenon. On the other hand, these other WR stars showed no evidence for broad features near their line center, whereas in γ^2 Vel, the wavelet spectrum suggests the existence of a uniform distribution of broad features (at a scale $\log \sigma_\xi(\mathrm{km\ s^{-1}}) \simeq 2.3$) over the whole profile. The scale of these features is reminiscent of the R-type LPVs found in the star HD 191765 (cf. Paper II), although we have no indication of a recursive behavior in γ^2 Vel.

The scaling properties of the variable components over the line profile are combined with the *wavelet power spectrum*, which yields the mean power in the wavelet spectrum within some interval $[\xi_1, \xi_2]$. The wavelet power spectrum, denoted $\langle \tilde{R}(\sigma_\xi) \rangle_{[\xi_1, \xi_2]}$ is obtained from

$$[\langle \tilde{R}(\sigma_\xi) \rangle_{[\xi_1, \xi_2]}]^2 \equiv \frac{1}{\xi_2 - \xi_1} \int_{\xi_1}^{\xi_2} \langle \tilde{R}(\xi, \sigma_\xi) \rangle^2 d\xi \,, \qquad (5)$$

and is analogous to the Fourier power spectrum. We present in Figure 3 the wavelet power spectrum of LPVs in γ^2 Vel in the interval $[\xi_1, \xi_2] = [-900, 900]$ km s^{-1}. The combined wavelet power spectrum from the two nights is compared with the wavelet power spectra from the LPVs in the C III λ5696 emission line in HD 192103 and from the LPVs in the He II λ5411 emission line in HD 191765 (see Paper II). The star HD 192103 is a single star with the same WR subtype as γ^2 Vel (WC8) and shows typical S-type LPVs as seen in most WR spectra. The star HD 191765, on the other hand, is a prototype, along with EZ CMa, for the rare class of WR stars with R-type LPVs.

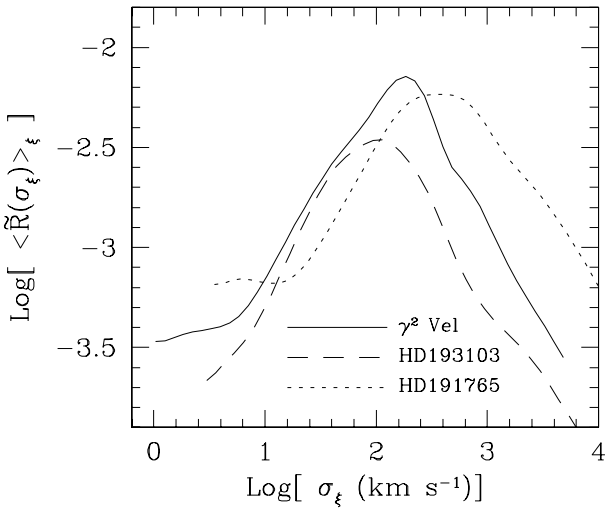

FIG. 3.—Wavelet power spectra from the LPVs found in the C III λ5696 emission line in γ^2 Vel (for both nights) are compared with the power spectra from the stochastic LPVs (narrow emission subpeaks) in the C III λ5696 from HD 192103, and the power spectra from the recursive LPVs (broad emission subpeaks) found in the He II λ5411 of HD 191765. The wavelet power spectrum from γ^2 Vel is apparently intermediate between these two other stars, suggesting the presence of both narrow and broad components.

One sees that γ^2 Vel seems to be intermediate between HD 192103 and HD 191765. Compared to HD 192103, γ^2 Vel definitely shows an excess of large-scale components [$\log \sigma_\xi(\mathrm{km\ s^{-1}}) \simeq 2$–3]. The star HD 191765 shows more power at the large-scale end but has a deficit in small-scale intrinsic features [$\log \sigma_\xi(\mathrm{km\ s^{-1}}) \simeq 1$–2] at the same time. This is not the case for γ^2 Vel, whose subpeak features show high levels of variability on both small and large scales.

3.2. *Wavelet Filtering*

The wavelet transform can be used to devise a very efficient scale-filtering tool. A spectral time series $R(\xi, t_i)$ can be recovered from its wavelet transform $\tilde{R}(\xi, \sigma_\xi, t_i)$ from the so-called *wavelet reconstruction theorem*, which for our specific choice of wavelet and normalization can be shown to be obtained easily from

$$R(\xi, t_i) = \int_0^\infty \tilde{R}(\xi, \sigma_\xi, t_i) \frac{d\sigma_\xi}{\sigma_\xi} \,. \qquad (6)$$

A scale filtering of the signal is obtained if, instead of rebuilding the signal from all its scale components, one integrates over a finite scale domain $[\sigma_{\xi 1}, \sigma_{\xi 2}]$:

$$R_{[\sigma_{\xi 1}, \sigma_{\xi 2}]}(\xi, t_i) = \int_{\sigma_{\xi 1}}^{\sigma_{\xi 2}} \tilde{R}(\xi, \sigma_\xi, t_i) \frac{d\sigma_\xi}{\sigma_\xi} \,. \qquad (7)$$

This procedure effectively filters out all signal components with characteristic scales out of the range $\sigma_{\xi 1} < \sigma_\xi < \sigma_{\xi 2}$.

We have defined four scale domains, each spanning a factor of 8, for the analysis of the γ^2 Vel spectral time series: A = [0.78, 6.3] km s^{-1}, B = [6.3, 50] km s^{-1}, C = [50, 400] km s^{-1}, and D = [400, 3200] km s^{-1}. These domains were not selected arbitrarily, but defined in such a way as to obtain a *natural* separation of the apparent scale components in the signal, as suggested from the wavelet power spectrum. We have plotted in Figure 4 the mean wavelet power spectrum for each night, along with the power spectrum for each of the four filtered components obtained with filters A, B, C, and D. One sees that the wavelet power spectrum of the original data can be viewed as a combination of four "bumps," which are separated from one another with our choice of wavelet filters. Note that the wavelet power spectrum of each filtered component does not fall abruptly at the band limits, although the filter bands are strictly defined. This is actually a very interesting by-product of the wavelet transform: it minimizes the numerical artifacts that can arise in Fourier bandpass filtering. This is made at the expense of the scale resolution and results in some leaking of power from one scale component to the next.

The time series for the filtered LPV patterns are presented in Figure 5. Note that the sum of the four scale components R_A, R_B, R_C, and R_D yields back the unfiltered time series. From examination of the variation patterns for each scale regime, it seems that we have achieved a reasonably good separation between instrumental fluctuations (scale domains A and D) and intrinsic stellar variability (scale domains B and C).

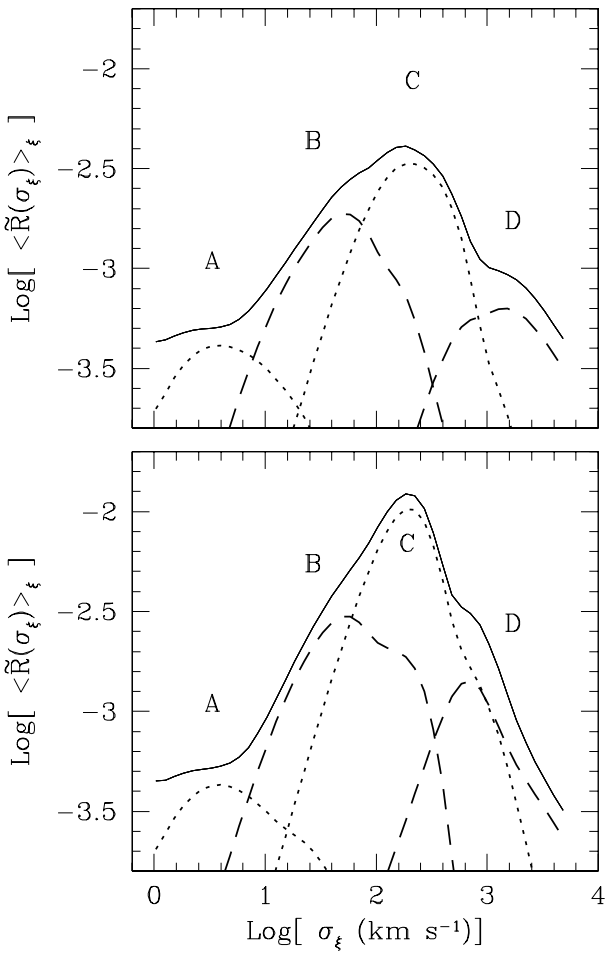

FIG. 4.—Wavelet power spectrum from each of the spectral time series (*top*, first night; *bottom*, second night) of residuals from γ^2 Vel (*solid line*), and from each of the corresponding, scale-filtered time series (cf. Fig. 5). The four filters separate the power spectrum in a seemingly *natural* way, i.e., along the four apparent bumps. The difference in the scaling properties of the LPV between the two time series can be explained mainly by a change in the amplitude of components sensitive to filter C. Note how the wavelet filtering yields a smooth separation of the scale components.

Spectral variations in scale domain A comprise the pixel-to-pixel variations that arise from photon-counting statistics, but also from other instrumental effects and contamination by cosmic rays and telluric lines. In the first night, one also sees the emergence of a weak Fabry-Perot (FP) pattern, which must have resulted from internal reflections in the instrument. The fact we detect this FP pattern in these difference spectra suggests that the pattern *varied* during the first night for reasons that are still unclear. The FP pattern probably remained stable in the second night, which explains why it does not show in $R(\xi, t_i)$. Finally, one can also see a trace of narrow *intrinsic* features near the center of the emission line that are absent from the edges. Their presence is more conclusive in the data from the second night, which is not contaminated by a variable FP pattern.

Variability in scale domain D reveals the presence of global, random variations in the line amplitude during the first night. These are likely due to errors in spectral rectification. As mentioned in § 2, we were obliged to define a pseudocontinuum using narrow spectral regions near the edges of the detector array. Apparently, these regions were affected either by intrinsic line variability or, more likely, by instrumental fluctuations, which resulted in spurious, vertical shifts in this pseudocontinuum. As a result, the intensity in the emission line seems to vary abruptly in the course of the night. In the second night, on the other hand, the filtered component $R_D(\xi, t)$ suggests a systematic shift in the radial velocity of the emission line during the night, which might be real or arise in small, systematic errors in the wavelength calibration. In any case, all these effects are relatively small compared with the intrinsic LPVs, which are obvious in scale domains B and C.

The regularity in the behavior of variable features at scale domains B and C, their strong correlation with location on the emission-line profile, and their symmetrical distribution around $\xi = 0$, all point to the intrinsic nature of these variable components. We note that the kinematics of broad (scale C) and narrow (scale B) features are not significantly different. Both components exhibit a behavior that is consistent with the same rate of motion on the line, suggesting that they arise from wind components having the same radial acceleration. This suggests that both narrow and broad line features are formed in similar dynamical regions of the wind. We will now show that these LPVs can be reproduced with a model of inhomogeneities in a radially expanding wind.

4. COMPARATIVE ANALYSIS

4.1. *Simulations of LPVs from an Inhomogeneous Wind*

We model the C III λ5696 LPVs in γ^2 Vel using the phenomenological working model introduced in Paper II, which describes the LPVs in terms of inhomogeneities in a radially expanding stellar wind. We provide here a brief summary of the model; the reader should refer to Paper II for more details.

The emission line is assumed to arise from a number of discrete wind emission elements (DWEEs). We assume the DWEEs to propagate radially along a monotonically increasing velocity law of the form

$$v_r(r) = v_\infty\left(1 - \frac{R_*}{r}\right)^\beta , \tag{8}$$

i.e., the so-called β-law, which is commonly used in models of WR winds (e.g., Schmutz 1997; Hillier & Miller 1998; Hamann & Koesterke 1998). The parameter R_* should be of the order of the stellar hydrostatic core radius, while β values in the range $0.5 < \beta < 4$ are typically used in the literature.

The relative emission f_e from one DWEE depends on its distance from the star, which can be expressed by the magnitude of its velocity v_r relative to the center of the star, yielding an emission function

$$f_e(v_r)dv \propto \exp\left[\frac{-(v_r - v_e)^2}{\sigma_{v_e}^2}\right] dv . \tag{9}$$

The parameters v_e and σ_{v_e} define the mean location and extension of the line emission region (LER) in wind velocity space, respectively.

We have shown in Paper II (see also Brown et al. 1997) that, in the optically thin case, we can use the shape of the emission-line profile to estimate the line emission as a function of the radial velocity in the wind. The mean line profile $\overline{S}(\xi)$ gives the emission as a function of projected velocity ξ.

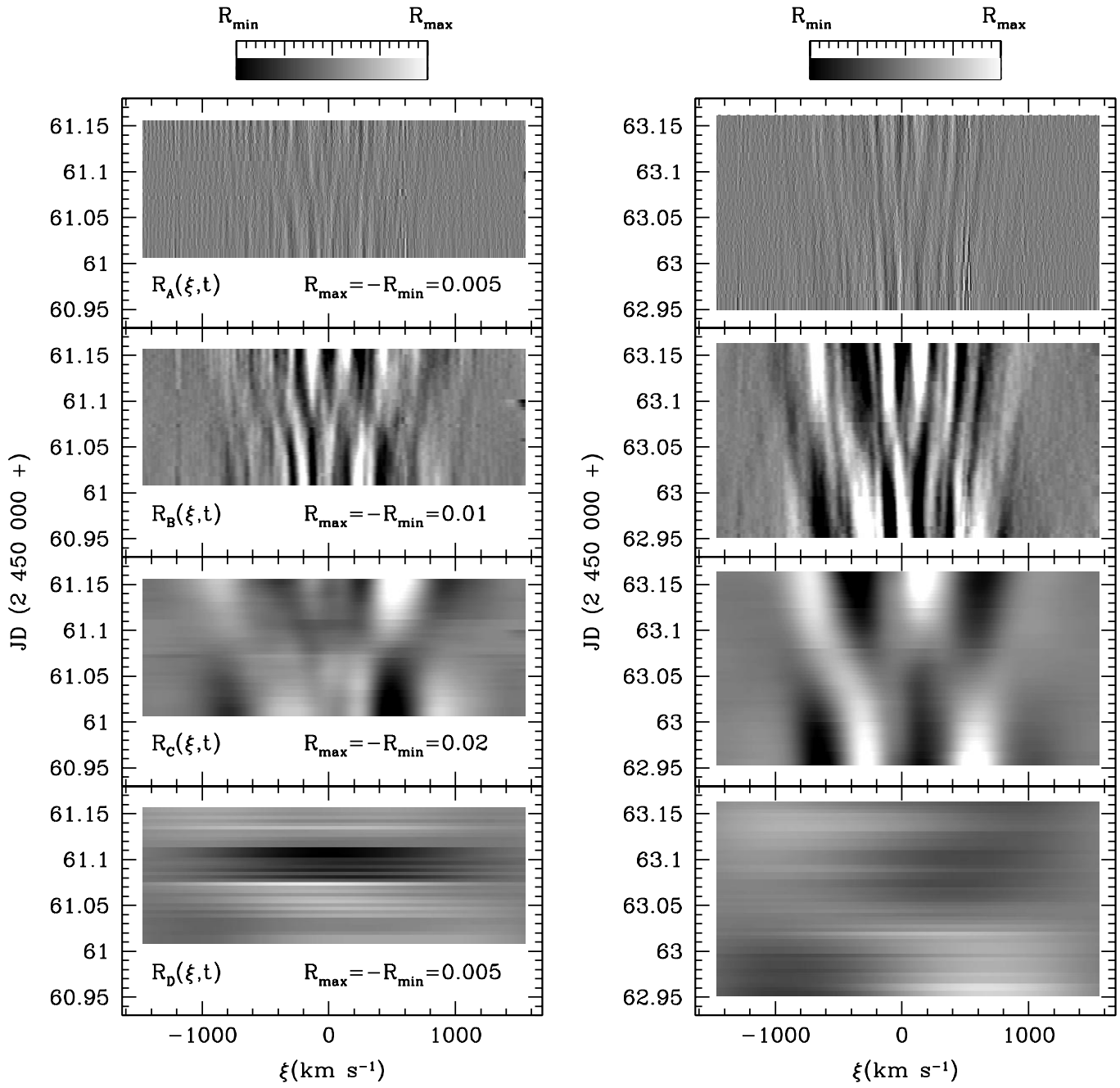

FIG. 5.—Wavelet filtering of the residuals using the four filters A, B, C, and D (from top to bottom, respectively), defined in § 3.2. The small-scale residuals R_A emphasize instrumental noise features, while R_B and R_C show the narrow and broad intrinsic moving subpeaks, respectively. The larger scale residuals R_D show what appear to be global variations in the emission-line profile.

From $\overline{S}(\xi)$, we can obtain the spherical deprojection, i.e., the emission as a function of radial velocity $F_e(v_r)$ as

$$F_e(v_r) \propto \left[-\xi \frac{d}{d\xi} \overline{S}(\xi) \right]_{\xi = v_r} . \tag{10}$$

This function is distinct from the function $f_e(v_r)$, because it depends on the radial velocity dispersion σ_{v_r} ("turbulent" motions) in the wind as well as on the extension of the LER, σ_{v_e}, in the wind *mean* velocity space:

$$F_e(v_r)dv \propto \exp\left[\frac{-(v_r - v_e)^2}{\sigma_{v_e}^2 + \sigma_{v_r}^2} \right] dv . \tag{11}$$

This can yield an estimate of σ_{v_e}, provided that σ_{v_r} can be evaluated by other means. The function $F_e(v_r)$ computed from the C III λ5696 emission line in γ^2 Vel is shown in Figure 6, where it can be compared with $F_e(v_r)$ obtained from the same emission line in the star HD 192103 (cf. Paper II). The range in radial velocity appears to be broader for γ^2 Vel. This suggests either the presence of larger perturbations (σ_{v_r}) in the velocity field, or a larger extension (σ_{v_e}) of the LER in mean bulk velocity space. Since both stars are of the same subtype (WC8) and have almost identical terminal wind velocities ($v_\infty \simeq 1415$ km s^{-1} for γ^2 Vel, and $v_\infty \simeq 1405$ km s^{-1} for HD 192103, according to Prinja et al. 1990), then it is reasonable to assume that the

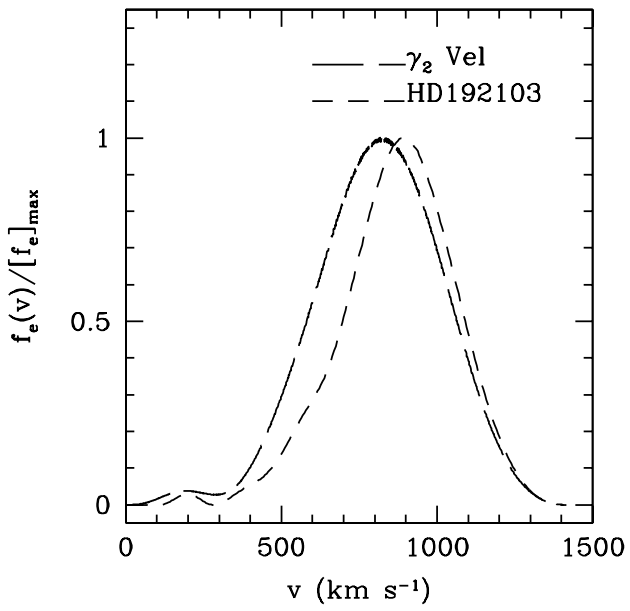

FIG. 6.—Estimated emission $F_e(v_r)$ from the C III λ5696 line as a function of the expansion velocity of emitting wind material, as estimated from the shape of the emission-line profile. The function $F_e(v_r)$ for γ^2 Vel (*long-dashed line*) is compared with $F_e(v_r)$ obtained from the same line in the WR star HD 192103 (*short-dashed line*), which is of the same WR subtype (WC8). The C III line emission apparently arises from a slightly broader velocity regime in γ^2 Vel.

location and size of the LER should be very similar. Therefore, the larger emission-line broadening in γ^2 Vel should be interpreted as evidence for larger σ_{v_r}. This interpretation is consistent with the observation of broader LPV subpeaks on the line profile, suggesting the existence of larger "turbulent" motions in some regions of the wind.

In our model, we assume a statistical distribution in the relative fluxes from DWEEs in the form of a power law:

$$n(f) \propto f^{-\alpha}, \quad f_0 < f < \eta f_0 . \tag{12}$$

We define N_e as the mean number of DWEEs that lie in the velocity regime $v_e - \Delta v_e < v_r < v_e + \Delta v_e$, where most of the emission occurs, and F_e as the mean value of the total emission from all DWEEs.

The DWEEs are assumed to have large intrinsic velocity dispersions, which are assumed to be anisotropic. We define a radial velocity dispersion σ_{v_r} and an azimuthal velocity dispersion σ_{v_θ}. The resulting line-of-sight velocity dispersion σ_ξ from one DWEE, therefore, depends on it projection angle $\mu = \cos\theta$:

$$\sigma_\xi^2 = \mu^2 \sigma_{v_r}^2 + (1 - \mu^2)\sigma_{v_\theta}^2 . \tag{13}$$

Because DWEEs with different values for μ will appear at different locations on the emission-line profile, the anisotropic velocity dispersion means that the width of the resulting LPV subpeaks will depend on their location on the line profile. Similarly, we separately define f_r as the escape probability in the radial direction and f_θ as the escape probability in the azimuthal direction. The relative escape probability f becomes:

$$f^2 = \mu^2 f_r^2 + (1 - \mu^2) f_\theta^2 . \tag{14}$$

The LPVs in other WR stars were found in Paper II to be consistent with $\sigma_{v_r} \simeq 4\sigma_{v_\theta}$ and with $f_r \lesssim f_\theta$.

We present in Figure 7 a model simulation that is in qualitative agreement with the data. Values for the model parameters used in these simulations are listed in Table 1. We used the same template as the data for sampling of the time series in order to facilitate the comparison with the data and to avoid sampling biases in the comparative analysis. Instrumental noise was implemented in the simulations in the form of random fluctuations according to Poisson statistics. One sees that the general appearance of the LPVs is reproduced remarkably well.

4.2. *Multiple LPV Modes*

We have performed several simulations using different values for the scale and amplitude of the wind fluctuations. We used the wavelet power spectrum $\langle \tilde{R} \rangle_\xi$ to compare the scaling properties of the LPVs from the simulations with that of the data. Figure 8 (*top*) show the $\langle \tilde{R} \rangle_\xi$ from simulations made with a single population of low velocity dispersion DWEEs (*a*) with $\overline{\sigma}_\xi = 80$ km s^{-1}. Although there is considerable scatter in $\langle \tilde{R} \rangle_\xi$, it is clear that these simulations cannot fully reproduce the $\langle \tilde{R} \rangle_\xi$ from the data. The simulations definitely lack some power in the scale range $2 < \log \sigma_\xi(\text{km s}^{-1}) < 3$. This can be compensated for if we add an extra population of high velocity dispersion DWEEs (*b*) with $\overline{\sigma}_\xi = 200$ km s^{-1}. The LPVs resulting from population *b* cannot account for the observed $\langle \tilde{R} \rangle_\xi$ alone (*middle*). However, simulations made by summing patterns from populations *a* and *b* results in wavelet power spectra

TABLE 1

PARAMETER OF THE INHOMOGENEOUS WIND MODEL AND BEST-FIT VALUES

Parameter	Description	Component *a*	Component *b*
v_∞	Terminal wind velocity	1400 km s^{-1}	1400 km s^{-1}
R_*	Velocity law parameter (physical size)	10 $R_\odot$	10 $R_\odot$
β	Velocity law parameter (β-law index)	4	4
v_e	Location of emission region (in radial velocity space)	850 km s^{-1}	850 km s^{-1}
σ_{v_e}	Extension of emission region	150 km s^{-1}	150 km s^{-1}
F_e	Total flux (equivalent width)	1500 km s^{-1}	400 km s^{-1}
N_e	Mean number of discrete elements	5000	25
α	Flux distribution parameter (power index)	3	3
η	Flux distribution parameter (range)	10^2	10^3
σ_{v_r}	Local velocity dispersion ($\parallel$ to propagation)	160 km s^{-1}	200 km s^{-1}
σ_{v_θ}	Local velocity dispersion ($\perp$ to propagation)	40 km s^{-1}	200 km s^{-1}
f_r/f_θ	Escape probability ratio	0.7	1.0

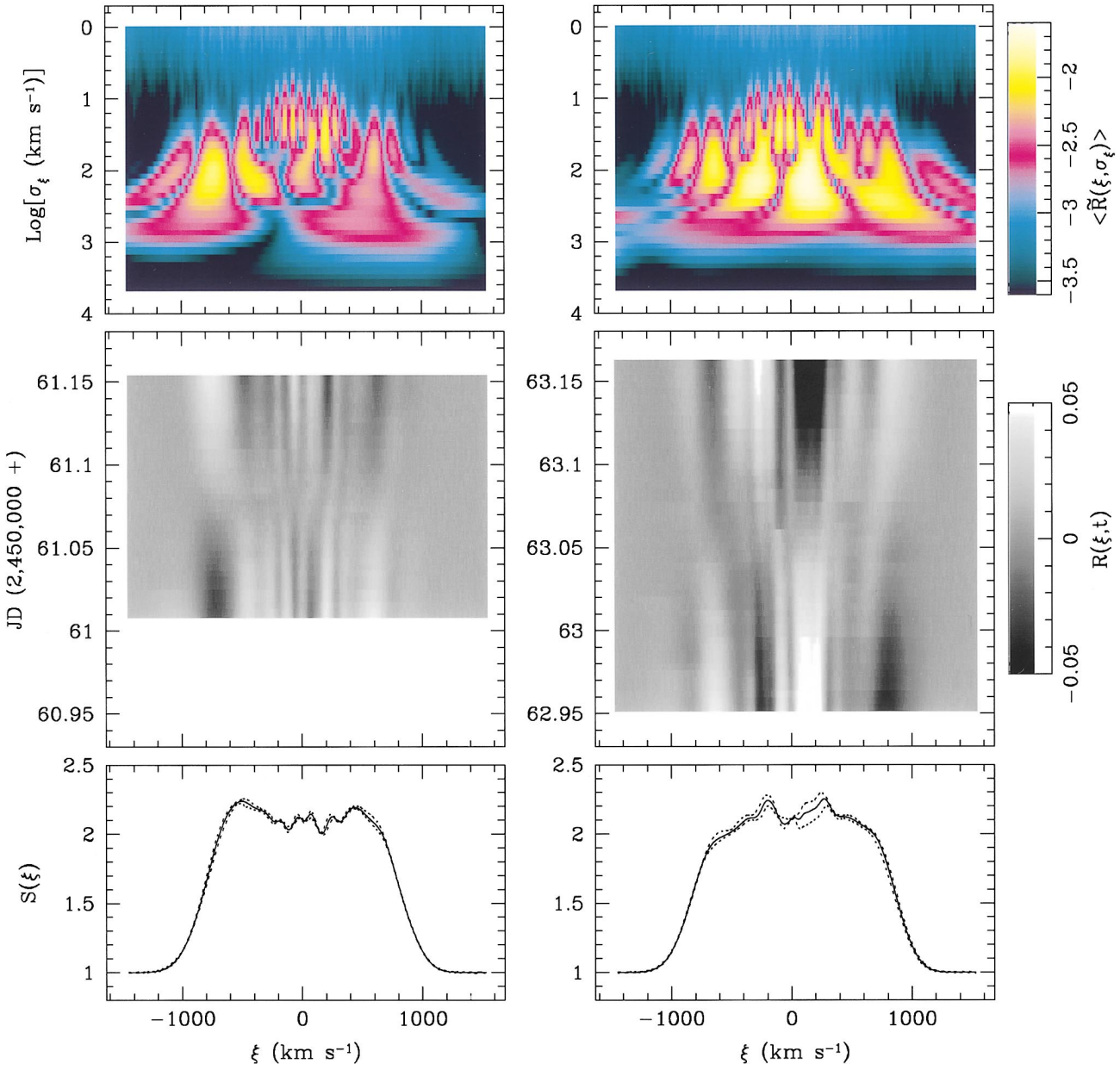

FIG. 7.—Simulation of the variability in the C III λ5696 emission line from an inhomogeneous wind, using the same time-series template as the data. Values of the model parameters are listed in Table 1. The gray-scale plots shows the residuals obtained after subtracting off the mean profile (*bottom*); the color plots show the corresponding mean wavelet spectrum. The resulting LPV patterns are very similar to those seen in the data in both general appearance and scaling properties (cf. Fig. 1).

that are in good agreement with those from the data (*bottom*).

This two-component solution is not unique: the shape of the wavelet spectrum could be reproduced using a more complex distribution of subpeaks on many more different scales. However, the two-component solution provides an easy explanation for the fact that the LPVs from γ^2 Vel differ from those of other WR stars: the difference is in the existence of an extra component of high velocity dispersion DWEEs. Moreover, whereas we used the same amplitude for component *a* to fit the wavelet power spectrum from each of the two data sets, we had to use a different amplitude for component *b*. This suggests that the first population is relatively stable, while the second population is subjected to a significant night-to-night change in amplitude.

We note that the amplitude of the variability resulting from one population of DWEEs can be increased in at least two independent ways: (1) by increasing the mean flux F_e arising from this component; and (2) by decreasing the mean number N_e of DWEEs responsible for the emission. For a given statistical flux distribution of DWEEs (i.e., fixed values of η and α; cf. § 4.1), the amplitude $\sigma_{\rm LPV}$ of the LPV is expected to be $\sigma_{\rm LPV} \propto F_e N_e^{-1/2}$. For a single population of DWEEs, it is possible to get an estimate of N_e from measured values of F_e and $\sigma_{\rm LPV}$. However, in the case where there are two distinct components responsible for line emission, although we may estimate the $\sigma_{\rm LPV}$ from each component with $\langle \tilde{R} \rangle_\xi$, we know only the sum of the mean flux from each component $F_{\rm ea} + F_{\rm eb}$. Therefore, it is not possible to estimate $N_{\rm ea}$ and $N_{\rm eb}$ from $\sigma_{\rm LPV}$, even with the help of the wavelet power spectrum.

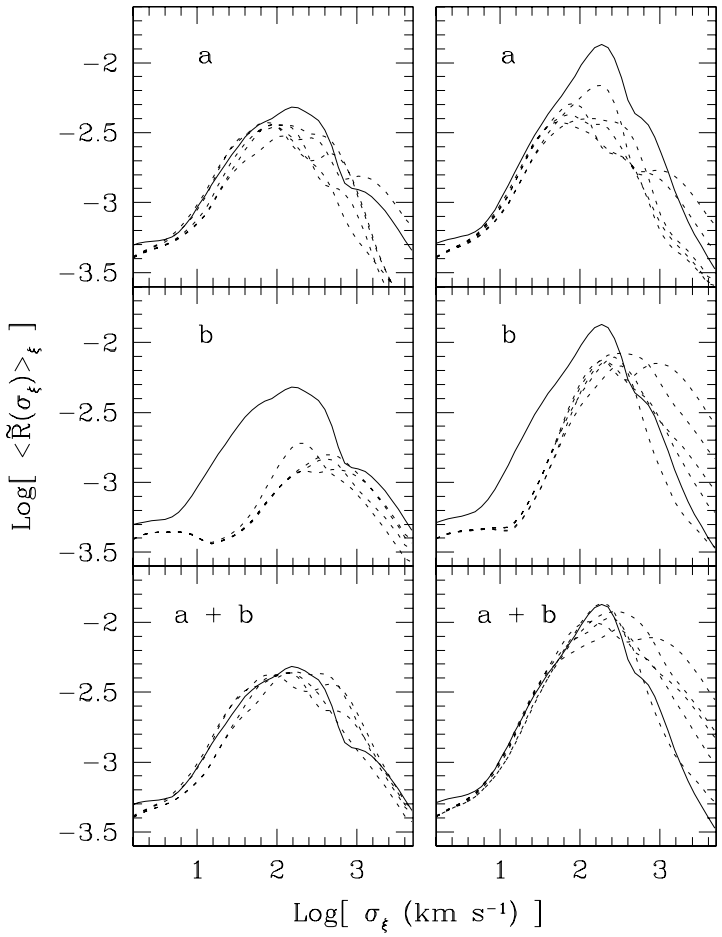

FIG. 8.—Comparison between the wavelet power spectrum from the γ^2 Vel data (*solid lines*), with the wavelet power spectra from simulations (*dotted lines*). The top panels compare the data with simulations made to generate LPV patterns similar those seen in most WR stars, showing narrow ($\bar{\sigma}_\xi \simeq 80$ km s^{-1}) stochastic subpeaks (*a*). Middle panels show the resulting wavelet power spectra from a set of broader ($\bar{\sigma}_\xi \simeq 200$ km s^{-1}) subpeak features (*b*). The best fit of the wavelet power spectra from γ^2 Vel is obtained from the superposition of the usual component with a extra set of broad emission features (*a* + *b*). The left column is for the first night of observation, and the right column for the second night. The apparent disagreement between data and simulations on large scales ($\log \sigma_\xi \gtrsim 3$) for the second night can be attributed to a filtering out of large scale features in the data reduction after the spectral rectification procedure.

If we assume that the mean flux from individual DWEEs is constant over time, then we have $F_e \propto N_e$, which also means that $\sigma_{\rm LPV} \propto N_e^{-1/2}$. Therefore we might expect to find a correlation between the total flux from one component (say, $F_{\rm eb}$) and the amplitude of the LPVs arising from this component. As it turns out, we observe that the apparent night-to-night change in the amplitude of component *b* correlates with the change in line equivalent width (EW), which is significantly larger in the second night. Though the correlation is only anecdotal, it is consistent with the idea that an increase in the amplitude of component *b* is responsible for both higher $\sigma_{\rm LPV}$ and increase in EW. This effect could actually be used to estimate the $F_{\rm ea}/F_{\rm eb}$ ratio, which would yield an estimate of $N_{\rm ea}/N_{\rm eb}$, although observations over many more nights would be required to test for this trend.

4.3. *Kinematics of the Inhomogeneities*

We have introduced in Paper II the *degradation function*, a numerical tool that can be used to estimate the radial acceleration of the wind from the systematic motion of LPV features. The degradation function $\sigma_D(a, \Delta t)$ of a spectral time series $R(\xi, t_i)$ is obtained from

$$[\sigma_D(a, \Delta t)]^2 \equiv \sum_{0<t_j-t_i<\Delta t} \int_{-v_e}^{v_e} \{R[\xi + a(t_j - t_i)v_e^{-1}\,\xi, t_i] - R(\xi, t_j)\}^2 [R(\xi, t_j)]^{-2} d\xi \,. \quad (15)$$

The degradation function compares one spectrum with another occurring at a subsequent time Δt after "stretching" the first spectrum in a way that mimics the motion in line-of-sight velocity component ξ of wind features having *radial* acceleration *a* with respect to the star. The minimum value for $\sigma_D(a, \Delta t)$ at a given Δt is obtained when $a \simeq a_r$, where a_r is the effective radial acceleration in the LER for the observed star (see Appendix B in Paper II). Experience shows that the best results are obtained when the intrinsic features in the signal are relatively narrow. This is because a motion at a given rate is more easily detected for narrow features. Experiments with the simulations have shown that better results are obtained if we use $R_B(\xi, t_i)$ to perform the degradation function, i.e., if we filter out all scales except those sensitive to the narrow components in the LPV patterns.

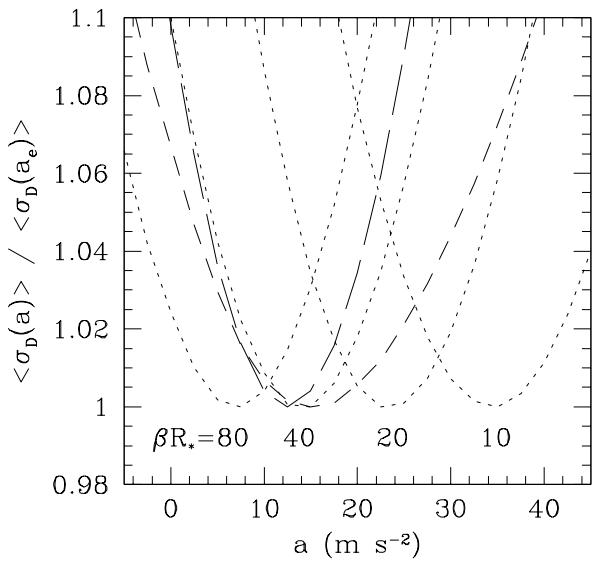

FIG. 9.—Estimate of the radial acceleration of inhomogeneous wind features from the degradation function $\langle\sigma_D(a)\rangle$ of the spectral time series (see § 4.3). The LPVs in γ^2 Vel (*dashed lines*) are consistent with propagating wind features with a radial acceleration $a = 13 \pm 3$ m s^{-2}, which can be fitted with β-type velocity laws having $\beta R_* \approx 40\ R_\odot$. Dotted lines show the degradation functions from simulations of LPVs arising in radially propagating wind inhomogeneities, and velocity fields defined by β-laws, with the indicated values of βR_*. The short dashed line is the degradation function for the JD 2,450,061 time series, while the long-dashed line is that for JD 2,450,063.

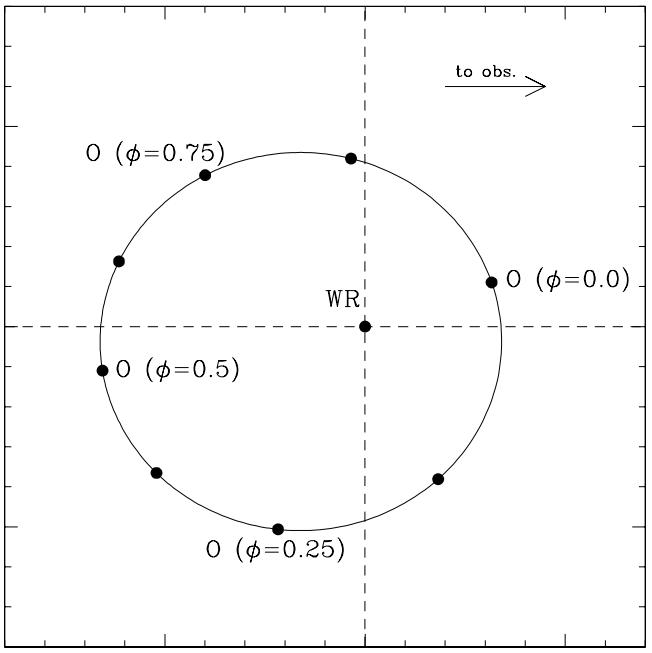

FIG. 10.—Schematic representation in the WR star rest frame of the orbital configuration of the γ^2 Vel system. The orbital inclination is not represented here. Spectroscopic observations presented in this paper were performed in the phase interval $0.26 < \phi < 0.29$.

We present in Figure 9 the mean degradation functions $\langle\sigma_D(a)\rangle$ obtained from all spectra separated by $\Delta t \leq 4$ hr. We compare the $\langle\sigma_D(a)\rangle$ for the LPV patterns in γ^2 Vel to the $\langle\sigma_D(a)\rangle$ from four simulations generated with different values of βR_*. We computed $\langle\sigma_D(a)\rangle$ on the wavelet filtered time series $R_B(\xi, t_i)$ and separately for each of the two nights for γ^2 Vel. We find that the motions of variable subpeaks in γ^2 Vel are consistent with radial accelerations $a_r \simeq 13 \pm 3$ m s^{-2}. The comparison with simulations reveals that such an acceleration in the C III λ5696 emission line is consistent with velocity laws having $25 < \beta R_*\ R_\odot^{-1} < 35$. One notes that $\langle\sigma_D(a)\rangle$ is broader for the first night (*short-dashed line*) than for the second one (*long-dashed line*). This reflects the larger uncertainty in estimating a_r in the first night, because of the smaller sample for a shorter time interval. We believe that one could get a very precise estimate of a_r from a larger sample.

In Paper II, we have used the degradation function to estimate the characteristic timescale of the subpeak features. We have tried to perform the same analysis on our γ^2 Vel spectral time series, but we could not obtain reliable estimates of the subpeak duration. The main reason for this failure is that the characteristic timescale of subpeak events is on the order of or larger than the size of our nightly samples.

4.4. *Comparison with the Orbital Phase*

We use the most recent ephemeris calculated for γ^2 Vel (Schmutz et al. 1997) to estimate the orbital phase at which our observations were performed. From a time of periastron passage $T_0 = 2{,}450{,}119.1$ (HJD) and an orbital period $P = 78.53$ days, we find orbital phases $\phi \simeq 0.26$ and $\phi \simeq 0.29$ for the first and second night of observation, respectively. The O star passes in front at phase $\phi = 0.03$, the WR star at phase $\phi = 0.61$. Since the orbit is eccentric ($e \simeq 0.33$) the WR star is then slightly in front of the O star at phases $\phi \simeq 0.26$–0.29 (see Fig. 10).

Because the momentum flux in the WR wind is much larger than that of its companion, the colliding-wind shock cone region wraps around the O star. At phase $\phi \simeq 0.27$, the mean flow in the shock cone region will be oriented roughly perpendicular to the line of sight (or slightly deviating if we take Coriolis effects into account). Therefore, any line emission from the shock cone at phase $\phi \simeq 0.27$ should appear in spectral region centered on $\xi \cong 0$. The opening angle θ of the shock cone has been evaluated based on X-ray observation of γ^2 Vel (Willis et al. 1995) as $20° < \theta < 30°$. The maximum spread $\Delta\xi$ in line-of-sight velocity of elements in the shock cone will be $\Delta\xi \simeq 2 \sin(25°) v_\infty \simeq 0.85 v_\infty$, where v_∞ is the terminal wind velocity, and it might be lower depending on the orbital inclination. Thus, assuming the flow in the shock cone to be similar to the mean wind flow, the effects of the shock cone on the emission-line profile should be restricted to a region no larger than $\Delta\xi \approx 1200$ km s^{-1}.

However, we detect broad features in the range -900 km s$^{-1} < \xi < 900$ km s^{-1} (cf. Fig. 1), which yields a $\Delta\xi \simeq 1800$ km s^{-1}. Even if we account for the large velocity dispersion associated with the variable subpeaks components ($\sigma_\xi \simeq 200$ km s^{-1}), the observed range in ξ is too large to be accounted for by emission features in the shock cone region. Therefore, the bulk of the line variability we see in γ^2 Vel must be intrinsic to the wind.

5. DISCUSSION

A first review on the observations showing evidence for line-strength variability in γ^2 Vel was presented more than 10 years ago (Jeffers et al. 1985). At that time, these were

interpreted as evidence for the presence of a compact companion, a hypothesis that has not been confirmed. Evidence for variability in the He II λ4686 line has been interpreted as evidence for irregular mass ejections (Taylor 1990). In this same work, observations of the C III λ5696 line strength were also presented, but unfortunately, the signal-to-noise ratio was not high enough to detect any variations on the scale we observed here. Line profile variations have been detected in UV lines of γ^2 Vel (Brandi et al. 1989; St.-Louis 1993). However we have found no report in the literature on the detection of LPV in optical emission lines, although their presence was rather suggestive in one study of the orbital variations using optical spectra (Moffat 1977), which included the C III λ5696 region.

There is little doubt that the variations we have detected in the C III emission-line profile in γ^2 Vel are intrinsic to the WR wind. Three observational arguments support this view: (1) the variability coincides with the whole spectral domain occupied by the C III λ5696 line emission; (2) the variability takes the form of intense emission subpeaks, which are significantly broader than pixel-to-pixel variations expected from instrumental noise and other contaminating effects; and (3) these subpeaks show organized patterns with a clear characteristic time behavior (motion from line center toward line edges). Possible causes of extrinsic variations are insignificant. Instrumental noise is low (S/N $\sim$ 2000) since we have observed a very bright star with a 3.6 m telescope. Line shifts can be ruled out, since they would only generate residual features near the line edges, whereas we also detect subpeaks near the line center. Only intrinsic variations in the line emission can explain the observed LPV patterns.

We believe that the observed LPVs arise primarily from inhomogeneities in the WR wind of γ^2 Vel. This is supported by the fact that (1) the LPVs occur in the same spectral domain as the line itself and (2) the systematic motion from the center toward the edges is consistent with a radial expansion. To verify this hypothesis, we have used the working model presented in Paper II and showed that it is possible to reproduce the LPV patterns in γ^2 Vel from a radially expanding, inhomogeneous wind, represented as the sum of a large number of discrete wind emission elements.

However, comparison between simulations and the data suggests that the LPV cannot be modeled using a single population of narrow discrete wind elements (with mean line-of-sight velocity dispersion $\overline{\sigma}_\xi \sim 80$ km s^{-1}), as is usually sufficient for most other WR stars. To reproduce the scaling properties of the LPV patterns in γ^2 Vel, we must use an extra set of broader ($\overline{\sigma}_\xi \simeq 200$ km s^{-1}) variable subpeaks, whose scale is reminiscent of the broad R-type LPVs observed in a few peculiar WR stars. The detection of these unusual, broad components comes as a surprise, because of their coexistence with the regular, narrow LPV subpeaks. In the stars where R-type LPVs were detected, there was no convincing evidence for the existence of narrow features.

One interpretation is that variable features of S-type and R-type always coexist, but their amplitude ratio changes from one star to another in such a way that one type usually dominates, while the other type remains unnoticed. Systematic spectroscopic monitoring of a larger sample of WR stars and their classification according to the scaling properties of their LPVs could shed more light on this idea. On the other hand, we have no evidence that the broad features in γ^2 Vel have a recurrent behavior, and it may be that this phenomenon is unrelated to the R-type LPV phenomenon. As it turns out, recent spectroscopic monitoring of γ^2 (Eversberg et al. 1998b) over several days has shown no evidence for any periodicity in the LPVs.

Another possible origin for the broad subpeak features of γ^2 Vel in C III λ5696 could be in the region where the wind from the WR star collides with that of its O companion (cf. St.-Louis 1993). We cannot attribute the broad component directly to LPVs of the P-type, because they occur on timescales much shorter than the 78.53 d orbital period. However, we believe that P-type LPVs arise from excess emission from the shock cone region, because of a correlation found between the EW of the C III λ5696 emission line and orbital phase (St.-Louis 1995). It seems likely that the shock cone region should be unstable and inhomogeneous (Stevens et al. 1992). In this case, the shock-cone emission could well be variable on timescales of minutes to hours and arise in the form of moving LPV subpeaks. Nevertheless, we have shown in § 4.4 that a shock-cone origin for the broad variable components is unlikely mainly because the range in line-of-sight velocities over which these features are observed is inconsistent with the predicted geometry of the shock cone.

However, we find anecdotal evidence that suggests that the amplitude of the broad LPV subpeaks is correlated with changes in the line EW. Since St.-Louis (1995) has found a correlation between EW and orbital phase, we are tempted to suggest that either (1) these EW variations with phase are not due to the shock cone emission, but rather due to the broad LPV subpeaks, whose effects are amplified when the orbital separation is low; or (2) that there are significant variations in EW associated with the broad LPV subpeaks, which are not phase-dependent, but which are superposed on the excess from the shock cone. This should be checked with high-resolution spectroscopic monitoring of γ^2 Vel spanning most of an orbital phase.

6. CONCLUSIONS

We have monitored the C III λ5696 emission line in the bright WR star γ^2 Velorum, in a search for line profile variations (LPVs) on short timescales (minutes to hours), at a very high signal-to-noise ratio. Observations reveal the presence of LPVs in the form of narrow moving subpeaks having a mean amplitude $\sim$5% of line intensity. These variable features appear to move systematically from line center toward line edges.

We have shown that the observed LPVs can be reproduced from a model of inhomogeneous features in a radially expanding stellar wind. We have used the working model presented in Paper II to make simulations of the LPVs in the C III emission line. A comparison between the data and the simulations reveals the LPVs in γ^2 Vel to be unusual. Whereas the LPVs in most WR star winds are in the form of relatively narrow ($\overline{\sigma}_\xi \simeq 80$ km s^{-1}), stochastic features (S-type), the LPVs in γ^2 Vel show the existence of an additional component of broader ($\overline{\sigma}_\xi \simeq 200$ km s^{-1}) variable features. These broad features are reminiscent of the broad recursive LPV features (R-type) occurring in a few peculiar WN stars (HD4004, EZ CMa, and HD 191765), although it is not possible to verify the existence of a recursive behavior with this data set. Independent longer time monitoring of γ^2 Vel has shown no evidence of recursive behavior so far (Eversberg et al. 1998b).

The C III λ5696 emission-line variability from γ^2 Vel is found to be affected by larger broadening effect than the same line in the star HD 192103, a WR star with the same subtype (WC8) and terminal velocity ($v_\infty \simeq 1400$ km s^{-1}). This is consistent with the existence of larger wind perturbations yielding higher velocity dispersions in γ^2 Vel, as reflected by the existence of the broad variable features.

We find that the motion of the narrow (S-type) features is consistent with a radial wind acceleration $a_r = 13 \pm 3$ km s^{-1}. If we assume that the wind has a velocity law in the form $v(r) = (1 - R_* r^{-1})^\beta$, the observed a_r is consistent with laws having $\beta R_* \simeq 40\ R_\odot$.

S. L. acknowledges the support provided by scholarships from NSERC of Canada and from FCAR of Québec. A. F. J. M. is grateful to the same two organizations and the Killam program of the Canada Council for the Arts for financial aid. T. E. thanks the Evangelisches Studienwerk/Germany for a three-year student bursary.

REFERENCES

Acker, A., Grosdidier, Y., & Durand, S. 1997, A&A, 317, L51
Balick, B., Rodgers, B., Hajian, A., Terzian, Y., & Bianchi, L. 1996, AJ, 111, 834
Brandi, E., Ferrer, O. E., & Sahade, J. 1989, ApJ, 340, 1091
Brown, J. C., Richardson, L. L., Cassinelli, J. P., & Ignace, R. 1997, A&A, 325, 677
Drissen, L., Robert, C., Lamontagne, R., Moffat, A. F. J., St-Louis, N., van Weeren, N., & van Genderen, A. M. 1989, ApJ, 343, 426
Eversberg, T., Lépine, S., & Moffat, A. F. J. 1998a, ApJ, 494, 799
Eversberg, T., Moffat, A. F. J., & Marchenko, S. 1998b, in preparation
Gayley, K. G., & Owocki, S. P. 1995, ApJ, 446, 801
Grafener, G., Hamann, W.-R., Hillier, D. J., & Koesterke, L. 1998, A&A, 329, 190
Hamann, W.-R., & Oesterke, L. 1998, A&A, 333, 251
Hamann, W.-R., Wessolowski, U., & Koesterke, L. 1994, A&A, 281, 184
Hillier, D. J. 1991, A&A, 247, 455
Hillier, D. J., & Miller, D. L. 1998, ApJ, 496, 407
Jeffers, S., Stiff, T., & Weller, W. G. 1985, AJ, 90, 1852
Langer, N. 1989, A&A, 210, 93
Lépine, S., & Moffat, A. F. J. 1999, ApJ, 117, in press (Paper II)
Lépine, S., Moffat, A. F. J., & Henriksen, R. N. 1996, ApJ, 466, 392 (Paper I)
Luehrs, S. 1997, PASP, 109, 504
Marchenko, S. V., Moffat, A. F. J., Eenens, P. R. J., Hill, G. M., & Grandchamps, A. 1995, ApJ, 450, 811
McCandliss, S. R., Bohannan, B., Robert, C., & Moffat, A. F. J. 1994, Ap&SS, 221, 155
Moffat, A. F. J. 1996, Rev. Mexicana Astron. Astrofis., 5 (38)
———. 1977, A&A, 57, 151
Moffat, A. F. J., Drissen, L., Lamontagne, R., & Robert, C. 1988, ApJ, 334, 1038
Morel, T., St-Louis, N., & Marchenko, S. V. 1997, ApJ, 482, 470
———. 1998, ApJ, in press
Nugis, T., & Niedzielski, A. 1995, A&A, 300, 237
Owocki, S. P., & Rybicky, G. B. 1991, ApJ, 368, 261
Pasquali, A., Langer, N., Schmutz, W., Leitherer, C., Nota, A., Hubeny, I., & Moffat, A. F. J. 1997, ApJ, 478, 340
Prinja, R. K., Barlow, M. J., & Howarth, I. D. 1990, ApJ, 361, 607
Robert, C., Moffat, A. F. J., Bastien, P., Drissen, L., & St-Louis, N. 1989, ApJ, 347, 1034
Robert, C. 1992, Ph.D. thesis, Univ. Montréal
Runacres, M. C., & Blomme, R. 1996, A&A, 309, 544
Schaerer, D., Schmutz, W., & Grenon, M. 1997, ApJ, 484, L153
Schmutz, W. 1997, A&A, 321, 268
Schmutz, W., et al. 1997, A&A, 328, 219
Stevens, I. R., Blondin, J. M., & Pollock, A. M. T. 1992, ApJ, 386, 265
St-Louis, N. 1995, IAU Symp. 163, Wolf Rayet Stars: Binaries, Colliding Winds, Evolution, ed. K. A. van der Hucht & P. M. Williams (Dordrecht: Kluwer), 388
St-Louis, N., Hill, G., Moffat, A. F. J., Bartzakos, P., & Antokhin, I. 1996, in Wolf-Rayet Stars in the Framework of Stellar Evolution, ed. J.-M. Vreux (Liège: Inst. d'Astrophys.), 331
St-Louis, N., Willis, A. J., & Stevens, I. R. 1993, ApJ, 415, 298
Taylor, M. 1990, AJ, 100, 1264
Vakili, F., Mourard, D., Bonneau, D., Morand, F., & Stee, P. 1997, A&A, 323, 183
van der Hucht, V. A., et al. 1997, NewA, 2, 245
Vreux, J.-M., Gosset, E., Bohannan, B., & Conti, P. 1992, A&A, 256, 148
Willis, A. J., Schild, H., & Stevens, I. R. 1995, A&A, 298, 549